Modelling the self-assembly of COPII outer coat

Ferran Gonzalez Hernandez[1]*, Buzz Baum[2], Andela Šarić[3], Joel Forster[1,3]

Abstract
An essential cellular process is the exchange of molecules (cargoes) between organelles. Coated proteins, such as the coat protein complex II (COPII), are responsible for such transport. The inner and outer coat of the COPII complex assemble to deform and cut the membrane of the endoplasmic reticulum (ER), generating vesicles that transport cargoes to the Golgi apparatus. Despite extensive research, the underlying physical mechanisms that control COPII assembly and the formation of vesicles are still not well understood. For this project, a coarse-grained model has been developed to study the self-assembly of COPII outer coat, which is constituted by Sec13-31 rod-shaped subunits. The model has been designed to investigate the key elements and molecular interactions that govern the self-assembly of these rods into different geometrical structures. In the simulations performed, the relevance of the parameters defining Sec13-31 rods have been analysed to better understand their role in outer coat assembly.

[1] *CoMPLEX, University College London, London, United Kingdom*
[2] *LMCB, University College London, London, United Kingdom*
[3] *Department of Physics, University College London, London, United Kingdom*
*__Ferran Gonzalez Hernandez__: ucbpfgo@ucl.ac.uk

Contents

1. Introduction

Eukaryotic cells contain a variety of membrane-bound organelles, each with specific roles and composition. Communication between different compartments is an essential process to maintain cellular structure and homeostasis. A wide variety of proteins and lipids (cargoes) are exchanged between organelles through different transport processes. Small membrane vesicles bud from an originating compartment and fuse with another to transport different molecules. These vesicles are formed by coat proteins, which recruit cargoes and induce the formation of buds in a membrane. Despite extensive research, the complex mechanisms by which coat proteins collect cargo, induce curvature in a lipid bilayer, coordinate the scission of buds and finally fuse with target membranes are still not fully understood [1].

Recent advancements in X-ray crystallography, Cryo-electron microscopy and Cryo-electron tomography techniques have enabled to characterize different structures involved in intracellular trafficking. The three main types of vesicle coat proteins are clathirn-coated vesicles (CVVs), coat protein complex II (COPII) vesicles, and COPI vesicles[1]. Despite differences in their composition and trafficking routes, they share similar mechanisms of assembly and transport. They all contain two layers, an inner coat that interacts with cargo and membrane, and an outer coat that assembles with the inner layer to deform the membrane and form cage-like structures [2].

1.1 COPII

In contrast to other vesicle coats, COPII does not require specialized GTPase to form spherical vesicles [3]. COPII coated vesicles are responsible for transporting newly synthesized cargoes from the endoplasmic reticulum (ER) to the Golgi apparatus [4]. COPII inner coat is formed by heterodimers of Sec23-24 proteins, which are recruited to the ER membrane by a GTPase (Sar1). Sec13-31 proteins form the COPII outer coat. These complexes polymerize to shape ER membrane

and form a pre-budding complex. Outer coat units interact with inner coat to generate a complete cage [3].

Both coats can assemble into a variety of structures, ranging from small dimers to regular lattices, spherical cages and tubular structures [4]. However, the mechanical properties of these structures, as well as the way by which they interact with each other are far from being well understood. Therefore, it is necessary to understand the physical rules that govern their assembly, giving rise to structural versatility and flexibility to coat membranes in different shapes and curvatures that can carry a range of cargoes .

1.2 Sec13-31 outer coat

Despite a lack of structural data for inner coat structure and assembly, recent studies have improved the understanding of Sec13-31 structure. Sec13-31rods are the assembly units of COPII outer coat. Cryo-electron microscopy techniques have enabled the study of the structure of these rods and the geometrical rules that govern their assembly into a variety of structures and cages. Two Sec13 and two Sec31 polypeptides assemble to form heterotetrameric rods as shown in Figure 1 [5].

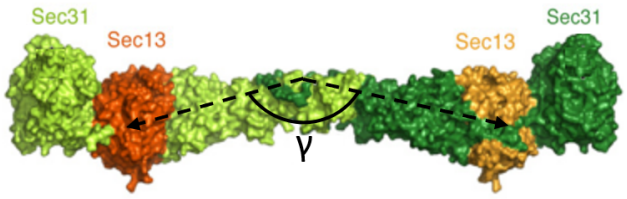

Figure 1. Sec13-31 heterotetramer. Figure adapted from [5].

Experimental studies have shown that Sec13-31 rods self-assemble into cuboctahedral cages (Figure 3), in which 24 Sec13-31 rods assemble to form the edges of the cage [6, 7]. Moreover, another geometrical structure is formed in vitro when outer coat proteins are mixed with Sec23-24, the icosidodecahedron [7]. Both structures show Sec13-31 rods disposed in a particular configuration (Figure 2).At each vertex of the cage, the ends of four different rods make contact forming a central hinge. As shown in Figure 2, each hinge contains two rods, the ends of which make central contact ('+ ends'), and two other rods, which ends are off-centred ('- ends'). Thereby, the ends of each rod are defined as '+' and '-' according to their relative position within the hinge.

The spatial conformation of the '+' and '−' ends give rise to the formation of 2 angles at each vertex: α (clockwise direction between '+' and '−' ends), and β (clockwise direction between '−' and '+' ends) [4]. While α has been observed to be 60° for all cages observed experimentally, β varies between 90° (cuboctahedral cages, Figure 2a) and 108° (icosidodecahedral cages, presence of inner coat Figure 2b) [4]. Stagg et. al. [7] suggested that the presence of membranes and cargoes would increase the resultant β angle, giving rise to the formation of different structures and curvatures.

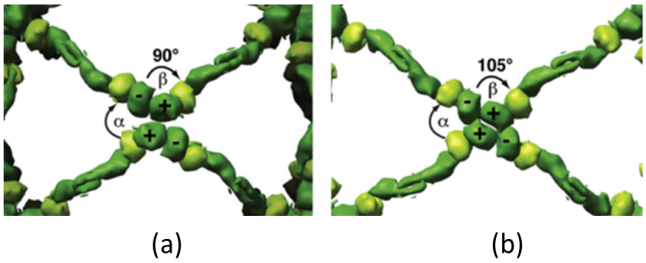

Figure 2. Illustration of the β angle differences on Sec13-31 hinges observed during experiments (a) without (b) with the presence of inner coat subunit. Noteworthy is that α and β are not in the same plane. Figure from [7].

Figure 1 shows an angle at the centre of the assembly unit. Bending at the centre of Sec13-31 has been observed to vary under different conditions. In studies where the assembly of outer coat units was performed without the presence of inner coat, a central angle of 135° and 165° was observed in humans and yeast respectively [8]. However, these angles seem to change with the presence of inner coat, membranes and cargo proteins, suggesting conformational changes that enable the formation of lattices and vesicles of different curvatures and sizes[8].

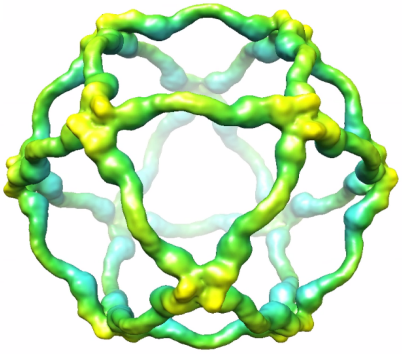

Figure 3. Reconstruction of Sec13-31 minimal cage. Figure from [8].

1.3 Context and experimental aims

Given the large number of molecules and interactions involved in COPII vesicle coat formation, this study aims to improve the understanding of the rules and properties concerning outer coat assembly. For this reason, the project starts with the initial goal of developing a 3D coarse-grained computational model that simulates the assembly and properties of COPII outer coat rods.

Although recent developments in experimental techniques have allowed researchers to improve the understanding of

these small-scale molecular systems, they still face many limitations. The presence of many intermediate structures and the high number of binding events that take place during the assembly of vesicle coat subunits, make experimental studies particularly challenging to perform and analyse. Consequently, over the last years, modelling and computational techniques have become more common in the study of the underlying characteristics controlling the assembly of macromolecules. Such simulations, allow a detailed control over those factors that play a critical role during the assembly process, providing a unique framework to simulate experiments and prove theoretical hypothesis.

In the field of vesicle coats, recent studies have already provided new insights into the mechanical properties of clathrin cages through coarse-grained simulations [9, 10]. For this reason, studies like this one represent novel and promising approaches towards a better understanding of the COPII machinery.

2. Methods

2.1 Model design

A computational model based on Sec13-31 rods was developed to study the self-assembly of COPII outer coat. For this project, interactions between Sec13-31 rods have been simulated without the presence of inner coat, lipid bilayer or cargo proteins. However, some of their structural effects on the outer coat can be analysed by changing the parameters that define these rods.

2.1.1 Sec13-31 rod design

Sec13-31 rods are the assembly units of the COPII outer coat. For this model, each rod has been defined by 6 spherical particles that form a rigid body (cp, Figure 4). To simulate attraction between rods, 3 ligands were placed at the extremes of each rod. One end contains 2 ligands (lg1, lg2), and the other has a single ligand (lg3). This configuration simulates the 'plus' and 'minus' ends of Sec13-31 rods observed experimentally (Figure 2).

The position of lg1 was aligned in the direction of the vector connecting both ends of the rod. Locations of lg2 and lg3 are specified by two parameters, β and α. As shown in Figure 4c, β represents the angle between a vector that goes from the first to the last central particle of the rod, and the vector that connects the core of the last central particle and the centre of lg2. The parameter α defines the position of lg3 relative to the vector that connects both ends of the rod (Figure 4b).

The parameter β is used to simulate the angle observed experimentally in Figure 2. For most of the experiments, β has been kept constant at 90°. However, the consequences of increasing the value of β have been analysed to study the possible effect of cargo proteins or membranes on outer rods coat assembly. α has been kept constant at 60° during all simulations performed in this study.

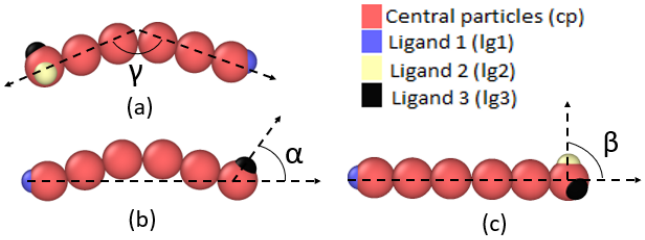

Figure 4. Model of Sec13/31 rod. a, b and c show γ, α and β angles in the plane formed by the 2 vectors presented in each case.

As shown in Figure 4a, γ defines the curvature of the rod. The structural effect of applying an angle at the centre of the assembly unit was studied in the experiments.

2.1.2 Rod Interactions

Attractive/repulsive forces between molecules were simulated by means of the Lennard-Jones (L-J) potential shown in Equation 1. The L-J potential is a common mathematical model used to approximate the interactions between neutral atoms or molecules. For molecular dynamic (MD) simulations, it is common to work with reduced units. All quantities reported in this study are expressed in standard reduced MD units [11].

$$V = 4\varepsilon\left[\left(\frac{\sigma}{r}\right)^{12} - \left(\frac{\sigma}{r}\right)^{6}\right] \qquad r < r_c \tag{1}$$

In Equation 1, ε represents the depth of the potential well (strength of the interaction between particles involved), σ is the finite distance at which the inter-particle potential is zero, and r is the distance between the centres of the interacting particles. As this potential is calculated for each particle present in the model, a potential cutoff (r_c) was also determined for the different molecules. By adjusting these parameters, the following interactions were specified (pairwise interactions not mentioned were considered null):

Interaction cp-cp In order to model an exclusionary volume for the central particles, their r_c was established at a distance of $\sigma \cdot 2^{1/6}$, generating a repulsive force when central particles were closer to each other than this distance. Their radius was established at 1 by specifying $\sigma = 2$. The strength of this interaction (ε) was settled at 100, which ensured that central particles did not overlap.

Interactions lg1-lg2, lg3-lg3 Attractive forces between lg1-lg2 and lg3-lg3 were modelled to approximate the assembly observed experimentally in Sec13-31 hinges (Figure 2). In order to avoid that many rods attached to one single ligand, their r_c and σ were determined at 2 and 1 respectively, creating a range of attraction of 1 around the ligand's surface. These values were kept constant during all the experiments performed in this study.

2.2 Coarse Grain Simulation

The model developed was implemented into LAMMPS, a molecular dynamics software broadly used for simulations in the field. The standard L-J potential was used to implement the attractions between molecules. All rods were subject to thermal motion simulated by Langevin dynamics, which provided damping and random noise to the movement of particles. Moreover, rods were treated as rigid bodies, allowing all molecules within each rod experience the same movement and rotation.

2.3 Design of experiments

2.3.1 Cage stability and rods assembly

To evaluate cage stability and determine the values for $\varepsilon_{lg3-lg3}$ and $\varepsilon_{lg1-lg2}$, 24 rods were placed at a close distance, each of them forming one edge of a cuboctahedral cage (Figure 6a). The simulations were performed to find $\varepsilon_{lg1-lg2}$ and $\varepsilon_{lg3-lg3}$ values that maintained the cage stable between 0 and 1 kT (expressed in reduced MD units, where k is the Boltzmann's constant and "$kT = 1$" is the room temperature), and generate disassembly of the cages above 1 kT (Figure 6c). This approach ensured that the strength of the interaction between rods allowed them to assemble at $1kT$, but other forces could still make them disassemble and affect the geometry of the structures generated.

In the next experiments, rods were randomly placed in the space and the role of density in their assembly was assessed during 1,000,000 time steps in a 200·200·200 3D space with boundary conditions at $1kT$. To do this, several initial rod densities were simulated to analyse the differences in emerging assembly patterns. In order to place rods randomly in the space, an additional script was written using Wolfram Mathematica software. There, an initial rod was defined at the centre of coordinates by specifying the location of its central particles and ligands. Next, a rotation matrix was applied to generate multiple rods in random directions, and they were then randomly placed within the specified space. Furthermore, an algorithm was developed to ensure that rods were kept at a minimum distance from each other to avoid them to overlap. To do this, each time a rod was randomly placed, an exclusionary prism determined by its extremes was calculated. Once the prism was defined, the algorithm checked that the following rods were not placed inside any already existing exclusionary prisms, ensuring in this way no overlapping between rods, consistent with the physical repulsive forces between central particles described above.

2.3.2 Rod bending and ligand's position

In the next set of experiments, the role of bent rods and ligand's position was assessed to study their impact on outer coat assembly. These experiments were performed by means of varying β and γ angles. Some specific values for β and γ have been observed experimentally, thus, we performed different simulations with $\beta = 90°$, $108°$ and $120°$ without bending. Then, values of $\gamma = 180°$, $165°$, $135°$ and $100°$ keeping $\beta = 90°$.

In order to have a significant number of observations, 5 repetitions were performed for each value of β and γ studied, in which the initial position of rods was random. All simulations were run during 1,000,000 time steps at 1 kT. Moreover, constant values for $\varepsilon_{lg1-lg2}$, $\varepsilon_{lg3-lg3}$ and density were used. Finally, at the end of each simulation, the geometrical coordinates of the molecules were outputted to perform posterior analyses.

2.4 Cluster analysis

Positional data generated during the simulations was outputted over time by LAMMPS, and later visualized with OVITO software. Qualitative and quantitative analyses of this data allowed to study cuboctahedral Sec13-31 cages under different temperature conditions as well as the structures formed by the assembly of rods randomly placed at the beginning of the simulation.

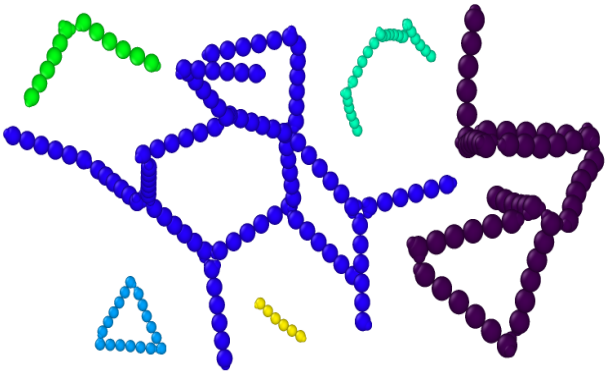

Figure 5. Illustration of the cluster analysis performed by the implemented algorithm. Snapshot of a simulation visualized with OVITO. Each rod was coloured according to its cluster identifier.

In order to numerically analyse the geometrical structures formed by the assembly of rods, a cluster analysis was performed. An algorithm was implemented to identify those rods that were assembled by calculating the distance between their respective ligands. Clusters were defined as sets of rods, each of which had at least one ligand within a cutoff distance (2.5) of another rod's ligand (Figure 5). If the ligands of a rod had no neighbours within a cutoff distance, then this was considered a single-rod cluster. Given a particular output, this analysis allowed to identify structures formed by the assembly of multiple rods, and calculate the number of rods present in each structure. Finally, geometrical characteristics of the assembled structures were visualized and compared using OVITO and Wolfram Mathematica.

2.5 Statistical analyses

For those simulations in which clusters were calculated, posterior statistical analyses were performed. First of all, the size of each cluster in a simulation was measured, and a histogram was plotted to visualize the distribution of cluster size. For all the simulations performed, the histograms showed a exponentially decreasing distribution, with a large number of rods forming clusters with only one or two rods. Data obtained from simulations with different β and γ angles was then compared. In order to deal with data that was not normally distributed, a Kruskal-Wallis test was initially applied to the different groups using R software. The Kruskal-Wallis test is a non-parametric test analogous to one-way ANOVA but it does not assume a normal distribution of the residuals. Moreover, due to the large number of tied values, an adjustment factor for tied ranks was applied by the software. When comparing various groups of data, the Kruskal-Wallis test works under the null hypothesis that the different groups come from identical populations. Then, for those analyses in which the p-value was significant (rejected the null hypothesis), a test for pairwise multiple comparisons between groups was performed using Conover-Iman test [12].

3. Results and Discussion

3.1 Cage stability and rods assembly

Different experiments were performed to evaluate the stability of the cage, each one at 0, 0.5, 1, 1.5 and $2kT$ during a relatively long time (100,000 time steps) for different $\varepsilon_{lg1-lg2}$ and $\varepsilon_{lg3-lg3}$ values. It is important to note that due to the time limitations of this study, the values were specified to fit logical ranges and known premises. However, further analyses would allow more accurate values and quantitative evaluation of the model's sensibility to these parameters.

First, it was detected that slightly higher attraction was necessary at the centre of the hinges (lg3-lg3) to sustain the cage. Therefore, an approximate ratio of $\varepsilon_{lg3-lg3}/\varepsilon_{lg1-lg2}$ was established at 1.2. Finally, stable cuboctahedral cages were achieved with $\varepsilon_{lg1-lg2}$ and $\varepsilon_{lg3-lg3}$ values of 15 and 18 respectively. For the rest of simulations performed in this study, both ε_s were kept at the values mentioned above. Figure 6 shows a simulation with these values, where temperature was progressively increased from 0 to $2kT$. It is clear how the simulated cage maintained its structure between 0 and $1kT$ but then rods started to disassemble at $1.5kT$ until the cage was completely melted at $2kT$. A video of the whole simulation is available at https://vimeo.com/255985904.

For simulations between 0 and $1kT$, the hinges of the cage still kept the structure observed experimentally (Figure 2), with two '+' and '-' ends. Flexibility in the hinges seemed to confer adaptability to the whole cage, maintaining its geometrical configuration while oscillating between different shapes.

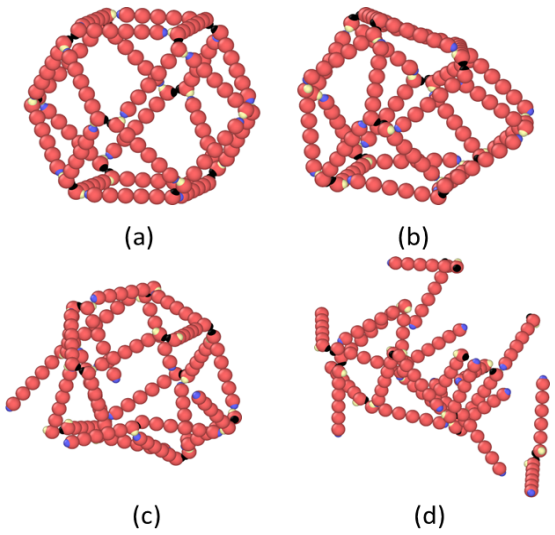

Figure 6. Sec13-31 cuboctahedral cage shapes under different temperature conditions. Each figure shows the state of the cage at: (a) 0, (b) 1, (c) 1.5 and (d) 2 kT.

Once the values for $\varepsilon_{lg1-lg2}$ and $\varepsilon_{lg3-lg3}$ were determined, the next set of experiments was carried out to asses rod density and their spontaneous assembly. With this approach, a set of initial simulations started with 100 rods randomly distributed. At the end of the simulation, many pairs of interacting rods were detected, as well as some tetrameric structures that resembled the hinges observed experimentally, but larger structures were not observed. When increasing the number of rods to 1,000, a very rapid aggregation occurred, generating a single large cluster with a lattice-form configuration. Finally, the effect of an intermediate density of 550 rods was studied. In these simulations, a progressive assembly of rods started showing different geometrical structures, ranging from triangles and squares to small lattices, which finally assembled into some bigger clusters. Figure 8 illustrates in blue one of the lattices detected in this simulation. Although cuboctahedral cages were not detected in this study, some enclosed structures and lattices were formed. The initial density of rods played a crucial role in the emerging geometrical structures. Therefore, more accurate studies on the density of rods and the parameters controlling their interactions may promote the formation of cuboctahedral cages.

3.2 Rod bending and ligand's position

The simulations in this study were run with constant $\varepsilon_{lg1-lg2}$ = 15 and $\varepsilon_{lg3-lg3}$ = 18. Moreover, the density of rods was kept constant at 550, since it was found to be an appropriate value to observe the progressive emergence of different structures. By using the clustering algorithm, the distribution of cluster sizes at the end of the simulation was observed to be exponentially distributed for all simulations performed in this section. Figure 7 illustrates the cluster size distribution at the end of a simulation with straight rods and $\beta = 90^\circ$.

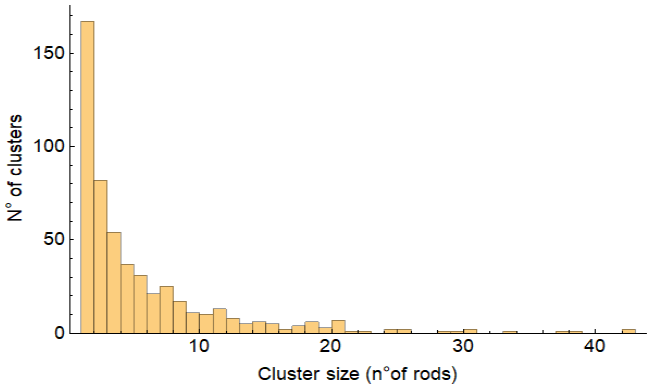

Figure 7. Histogram respresenting the distribution of cluster sizes at the end of the simulation. For this experiment β = 90° and γ = 180°.

It can be observed that there were a large number of single-rod clusters or dimers. However, a few large structures were also encountered in this simulation with more than 30 rods assembled.

In the following experiments, the role of central bending in the rod and the β angle observed experimentally were assessed.

3.2.1 Role of γ angle

In this section, different experiments were performed to analyse the influence of γ angle on rod's assembly. To do this, different simulations were computed with γ angles of: 180° (straight rods), 165 °, 135 ° and 100°. We selected these values as human and yeast Sec13-31 rods have shown angles of 135 ° and 165 ° respectively *in vitro*.

The sizes of the clusters at the end of the simulation were compared between groups that used different values for γ. First of all, the Kruskal-Wallis test gave a p-value of $3 \cdot 10^{-7}$, indicating that at least one of the groups came from a different population. Therefore, a Conover-Iman test for multiple pairwise comparisons was applied to analyse which groups showed significant differences.

Table 1. Conover - Iman test

Pairwise comparison	Statistic	Pr(>||)
180°-165°	0.783	0.434
180°-135°	3.612	< 0.001
180°-100°	4.99	< 0.001
165°-135°	2.839	0.005
165°-100°	4.204	< 0.001
135°-100°	1.299	0.194

Table 1 shows that significant differences (considering p-value < 0.05) were detected in cluster size distribution between unbend rods and rods with γ angles of 135° and 100°, whereas results from rods with 180° and 165° were considered to come from identical populations. Moreover, significant differences were observed between simulations with γ angles of 165° and 135°, which values were taken from experimental data of yeast and human Sec13-31 rods. However, it is important to note that the high number of tied values can affect the outcome of the test. Therefore, although previous corrections for tied values were applied, a qualitative study of the geometries was also performed.

Figure 8 illustrates the largest structures found for each group of simulations. Although the number of rods present in these structures showed a great variance between simulations, it is observed how lattices formed by rods with 135° and 100° (green and red) look shorter than the ones with 165° and 180° (yellow and blue). Specific configurations resembling the experimental lattices were observed in the emergent structures of all simulations, except from the one with 100 ° bending, which showed extremely curved and agglomerated clusters. Interestingly, experiments with γ of 135°, showed a larger number of enclosed and curved structures than the other simulations.

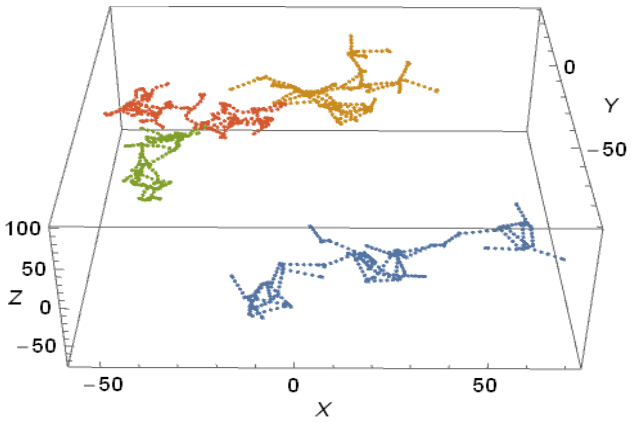

Figure 8. Graphical representations of the clusters detected with the largest number of rods for different values of γ: 180°(blue), 165°(yellow), 135°(green), 100°(red).

3.2.2 Role of β angle

Here, the relative position of lg2 was studied performing different sets of experiments with β: 90°, 108° and 120°. First of all, the number of rods per each cluster at the end of the simulation was calculated. Then, differences in cluster size were studied for the sets of experiments performed. The p-value for the Kruskal-Wallis was 0.232. Therefore, it cannot be considered that significant differences in cluster size distribution are present when applying β angles of 90°, 108° and 120°.

Despite the fact that significant differences were not detected in cluster size, it was observed that the biggest structures found during experiments with β angles of 108° and 120° contained 88 and 76 rods respectively, while for β = 90°

the maximum number of assembled rods was 42. Figure 9 illustrates these structures. It can be noticed that yellow (108°) and green (120°) lattices are much more elongated. Unlike the blue lattice (90°), quadratic and pentagonal geometries were present in lattices with higher β angle. Although the data generated did not provide enough evidence that these differences in structure are significant, further tests with larger samples might come to divergent conclusions. Simulations with higher number of rods in a larger space (constant density) could potentially have enough power to allow the assembly of more structures and show significant differences between the simulations with varying β angles.

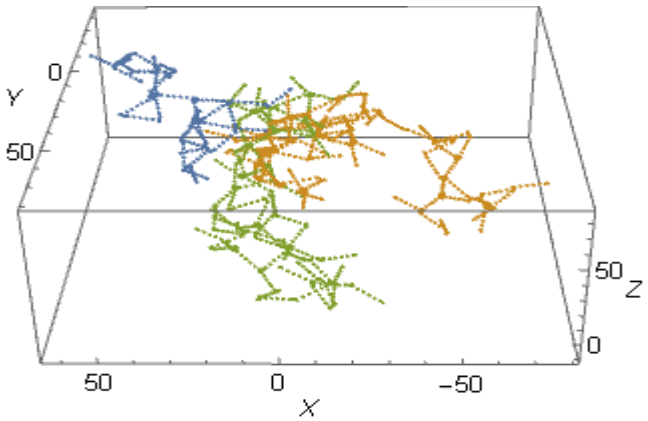

Figure 9. Graphical representations of the clusters detected with the largest number of rods for different values of β: 90°(blue), 108°(yellow), 120°(green).

4. Conclusions

The model developed in this project has enabled to study how some of the intrinsic properties of Sec13-31 rods affect the self-assembly of COPII outer coat. Results from cuboctahedral cages simulations showed that that flexibility of the hinges represented a crucial factor that allowed the full cage to change its shape while keeping its geometrical configuration under $1kT$. Moreover, it was detected that attractions between '$+'$ – '$+'$ (lg3-lg3) ends required a higher strength that '$+'$ – '$-'$ (lg1-lg2) to maintain the structure of the cage. This result supports hypothesis from recent studies analysing the contact regions at the vertices of COPII cages [8]. It was also found that the emergent geometries are highly sensible to the density of Sec13-31 rods. A specific number of rods was required to be present in a particular space to avoid the assembly of rods into either large single aggregates or small structures that did not assemble into lattices. This observation suggests a high control of COPII over the rods recruited into specific regions of the bi-lipid layer.

Another relevant finding has been the significant influence of γ angle in the self-assembly of outer coat subunits. The results from this study suggest that rods with different γ angles assemble into different emerging structures. Small changes in this angle (from 165° to 135°) seemed to be enough to affect the diversity of emergent structures assembled. Therefore, these results support that flexibility of Sec13-31 rods in this angle could be a mechanism to control the size of COPII vesicles depending on the carrying cargo.

Finally, results from simulations modifying β indicated that the role of this angle did not affect the size of the emergent structures detected at the end of the simulation. However, qualitative analyses showed that particularly big lattices were found with β angles of 108° and 120°. This fact indicates that further simulations with different conditions should be performed to better analyse the effect of this angle. Moreover, further development of the model would find more precise values for its parameters and probably induce the assembly of rods into the experimentally observed cages. Future projects could also introduce the inner coat and cell membrane into the model and analyse the complete assembly of COPII.

Acknowledgments

Prof. Buzz Baum and Dr. Andela Šarić for their constant guidance and fruitful meetings. Joel Forster for his extensive support and instruction through the project. Joshua Hutchings from the ISMB, for the meetings and conversations on COPII.

References

[1] Marco Faini, Rainer Beck, Felix T. Wieland, and John A G Briggs. Vesicle coats: Structure, function, and general principles of assembly. *Trends in Cell Biology*, 23(6):279–288, 2013.

[2] Frederick M. Hughson. Copy Coats: COPI Mimics Clathrin and COPII, 2010.

[3] D. Jensen and R. Schekman. COPII-mediated vesicle formation at a glance. *Journal of Cell Science*, 124(1):1–4, 2011.

[4] Giulia Zanetti, Simone Prinz, Sebastian Daum, Annette Meister, Randy Schekman, Kirsten Bacia, and John A G Briggs. The structure of the COPII transport-vesicle coat assembled on membranes. *eLife*, 2013(2), 2013.

[5] Stephan Fath, Joseph D. Mancias, Xiping Bi, and Jonathan Goldberg. Structure and Organization of Coat Proteins in the COPII Cage. *Cell*, 129(7):1325–1336, 2007.

[6] Scott M. Stagg, Cemal Gürkan, Douglas M. Fowler, Paul LaPointe, Ted R. Foss, Clinton S. Potter, Bridget Carragher, and William E. Balch. Structure of the Sec13/31 COPII coat cage. *Nature*, 439(7073):234–238, 2006.

[7] Scott M. Stagg, Paul LaPointe, Abbas Razvi, Cemal Gürkan, Clinton S. Potter, Bridget Carragher, and

William E. Balch. Structural Basis for Cargo Regulation of COPII Coat Assembly. *Cell*, 134(3):474–484, 2008.

[8] Alex J. Noble, Qian Zhang, Jason O'Donnell, Hanaa Hariri, Nilakshee Bhattacharya, Alan G. Marshall, and Scott M. Stagg. A pseudoatomic model of the COPII cage obtained from cryo-electron microscopy and mass spectrometry. *Nature Structural and Molecular Biology*, 20(2):167–173, 2013.

[9] M. Giani, W. K. Den Otter, and W. J. Briels. Early stages of clathrin aggregation at a membrane in coarse-grained simulations. *Journal of Chemical Physics*, 146(15), 2017.

[10] Matteo Giani, Wouter K. den Otter, and Wim J. Briels. Clathrin Assembly Regulated by Adaptor Proteins in Coarse-Grained Models. *Biophysical Journal*, 111(1):222–235, 2016.

[11] D. C. Rapaport. Molecular dynamics simulation of reversibly self-assembling shells in solution using trapezoidal particles. *Physical Review E - Statistical, Nonlinear, and Soft Matter Physics*, 86(5), 2012.

[12] Ronald L. Iman and W. J. Conover. The use of the rank transform in regression. *Technometrics*, 21(4):499–509, 1979.